24th COBEM - 2017

24th ABCM International Congress of Mechanical Engineering
December 3-8, 2017, Curitiba, PR, Brazil

COBEM-2017-0497
NON-ISOTHERMAL AEROELASTIC BEHAVIOR OF A TYPICAL SECTION WITH SHAPE MEMORY ALLOY SPRINGS

Vagner Candido de Sousa
Tarcísio Marinelli Pereira Silva
Carlos De Marqui Junior
Department of Aeronautical Engineering, Engineering School of Sao Carlos, University of Sao Paulo, Sao Carlos, SP, 13566-590, Brazil
vagner@sc.usp.br, tarcisio.silva@usp.br, demarqui@sc.usp.br

Abstract. *This paper addresses the modeling and analysis of a two-degree-of-freedom typical aeroelastic section with shape memory alloy (SMA) springs introduced through the pitch degree-of-freedom with a focus on exploiting the energy dissipating and damping capabilities of SMAs exhibiting pseudoelasticity. An augmented-state approximation to the Theodorsen aerodynamics is used for the determination of the aerodynamic loads. The phase transformation kinetics related to pseudoelasticity is based on Brinson's model. A heat transfer model is included to represent thermal effects such as Joule heating, natural convection, and latent heat associated with phase transformation. The effect of latent heat on the SMA temperature, on the critical stresses for phase transformation, and therefore on the overall aeroelastic behavior of the typical section is addressed. The electrical resistance of the SMA springs is expressed as function of the martensitic fraction and hence the corresponding variations in electrical activation are accounted for. The effects of the hysteretic behavior of the SMA springs on the aeroelastic behavior of the typical section are investigated at the flutter boundary and at post-flutter regime.*

Keywords: *shape memory alloy, pseudoelastic hysteresis, aeroelasticity, flutter, heat transfer*

1. INTRODUCTION

Aeroelastic phenomena such as flutter and limit-cycle oscillations (LCOs) are related to premature damage and failure of aeronautical structures. The literature on aeroelasticity includes studies on the use of smart materials in vibration control problems. Several research groups have investigated the use of piezoelectric materials in active and passive aeroelastic control cases in the last years (Giurgiutiu, 2000). Shape memory alloys (SMAs) have also been pointed out as promising materials for passive damping augmentation in mechanical and aerospace structures (Gandhi and Chapuis, 2002). The hysteretic response of shape memory alloys exhibiting pseudoelasticity provides energy dissipating and damping capabilities for these materials, and therefore, the effectiveness of the pseudoelastic behavior of shape memory alloys has been investigated for passive structural vibration control (Ibrahim, 2008). The effect of pseudoelasticity of SMA springs on the aeroelastic behavior of a typical section at the flutter speed and post flutter condition was also recently reported (Sousa and De Marqui Jr, 2014).

Sousa and De Marqui Jr (2014) present the modeling of a 2-DOF typical aeroelastic section with SMA springs introduced to the pitch degree-of freedom (DOF). Brinson's model is employed to describe the behavior of the SMA (Brinson, 1993), and the helical spring model follows reference (Liang and Rogers, 1997). This paper extends the work of Sousa and De Marqui Jr (2014) by including a heat transfer model (Faulkner *et al.*, 2000; Hadi *et al.*, 2010) to their original model of SMA springs. The unsteady aerodynamic loads (lift force and pitch moment) are obtained by Jones' exponential approximation to Wagner's indicial function cast in state-space representation (Jones, 1938; Edwards, 1977). The effects of pseudoelastic hysteresis of SMA springs on the aeroelastic behavior of the 2-DOF typical section are discussed from the dissipative standpoint for the flutter condition and above.

2. MODEL

2.1 Shape Memory Alloy Model

The critical stresses for phase transformation in SMAs are described in this paper by

$$\sigma_s^M = \sigma_s^{\min} + C_M \left(T - M_s\right) \tag{1}$$

$$\sigma_f^M = \sigma_f^{\min} + C_M\left(T - M_s\right) \tag{2}$$

$$\sigma_s^A = C_A\left(T - A_s\right) \tag{3}$$

$$\sigma_f^A = C_A\left(T - A_f\right) \tag{4}$$

where σ_s^M is the critical value of stress for the onset of stress-induced phase transformation (or forward transformation), σ_f^M is the critical stress for the completion of stress-induced transformation, σ_s^A is the stress value for the onset of the recovery of the austenitic phase (or reverse transformation) and σ_f^A is the stress value at which the austenitic phase is completely recovered. Additionally, $\sigma_s^{\min}$ and $\sigma_f^{\min}$ are minimum stresses at which stress-induced transformation begins and completes, respectively; C_M and C_A represent the influence of temperature on critical stresses for forward and reverse transformations, respectively; M_s is the martensite start temperature, A_s is the austenite start temperature and A_f is the austenite finish temperature (in the absence of stress); T is the SMA temperature (Brinson, 1993).

The martensitic fraction during forward transformation is given by

$$\xi^{\mathrm{A}\to\mathrm{M}} = \frac{1-\xi_0}{2}\cos\left[\frac{\pi}{\sigma_s^{\min}-\sigma_f^{\min}}\left(\sigma-\sigma_f^M\right)\right] + \frac{1+\xi_0}{2} \tag{5}$$

where ξ_0 is the initial martensitic fraction and when the applied stress increases from σ_s^M up to σ_f^M. On the other hand, the martensitic fraction during reverse transformation is given by

$$\xi^{\mathrm{M}\to\mathrm{A}} = \frac{\xi_0}{2}\left\{\cos\left[\frac{\pi}{A_f-A_s}\left(T-A_s^\sigma\right)\right]+1\right\} \tag{6}$$

when the applied stress decreases from σ_s^A to σ_f^A and where

$$A_s^\sigma = A_s + \sigma/C_A$$

is the temperature at which the austenitic phase begins to stabilize with applied stress (Brinson, 1993).

By using the principle of conservation of energy, the heat transfer model is presented as (Faulkner *et al.*, 2000; Hadi *et al.*, 2010)

$$m_s C_p \dot{T} = \frac{V^2}{R\left(\xi\right)} + m_s L_h \dot{\xi} - h_c A_c\left(T - T_\infty\right) \tag{7}$$

where m_s is the mass of the SMA spring, C_p is specific heat, V is voltage, R is electrical resistance of the SMA spring, h_c is convection coefficient, A_c is the circumferential area, T_∞ is ambient temperature, overdot denotes time derivative and L_h is the latent heat. The electrical resistance is expressed as function of the martensitic fraction by

$$R\left(\xi\right) = R_A + \xi\left(R_M - R_A\right) \tag{8}$$

where R_A and R_M are the electrical resistances of the fully austenitic and fully martensitic phases, respectively.

2.2 Aeroelastic Model with SMA Springs

The aeroelastic model is a 2-DOF (plunge and pitch displacements) typical section (Fig. 1(a)). The SMA springs are included in the pitch DOF (replacing to torsion spring of Fig. 1(a)) at the ends of a rigid shaft passing through the elastic axis of the typical section (Fig. 1(b)). The plunge and pitch displacement variables are h and α, respectively; b is the semichord length, x_α is the dimensionless distance from the elastic axis to the center of gravity, k_h is the plunge stiffness per unit length (in the span direction), k_α is the torsional stiffness per unit length (obtained from the SMA springs S_1 and S_2 in Fig. 1(b)), M_α is the aerodynamic pitch moment per unit length, L is the lift force per unit length, U_∞ is the airflow speed, m is the mass per unit length and m_f is a non-ideal extra mass per unit length in the plunge DOF.

The dimensionless equations of motion for the typical section with SMA springs in the pitch DOF are

$$r_\alpha^2\alpha'' + x_\alpha\bar{h}'' + \zeta_\alpha\alpha' + \vartheta\left(\alpha,\xi_1,\xi_2\right) = \bar{M}_\alpha \tag{9}$$

$$x_\alpha\alpha'' + \mu\bar{h}'' + \zeta_h\bar{h}' + \bar{h} = -\bar{L} \tag{10}$$

where $\bar{h} = hb^{-1}$ is the dimensionless plunge displacement, $\mu = (m+m_f)m^{-1}$ is the plunge-to-pitch mass ratio, $r_\alpha = (I_\alpha m^{-1}b^{-2})^{1/2}$ is the dimensionless radius of gyration, I_α is the moment of inertia per unit length, $\bar{t} = \omega_h t$ is a dimensionless time, where t is the dimensional time, $\omega_h = \left(k_h m^{-1}\right)^{1/2}$ and $\dot{x} = \omega_h x'$ and $\ddot{x} = \omega_h^2 x''$ are the time

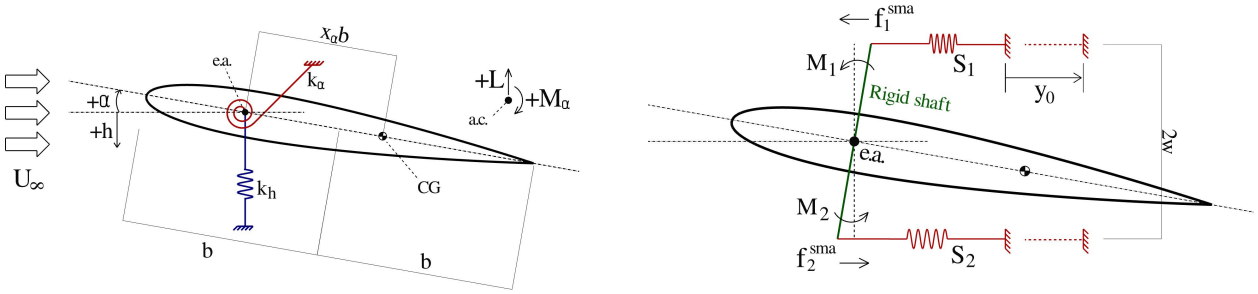

(a) (b)

Figure 1. Typical aeroelastic section (a) representation and (b) detail of the torsional stiffness design with SMA springs.

derivatives, the overdot and the prime denote differentiation with respect to t and $\bar{t}$, respectively, $\zeta_h = d_h(m\omega_h)^{-1}$ is the damping ratio of the plunge DOF and $\zeta_\alpha = d_\alpha(mb^2\omega_h)^{-1}$ is the damping ratio of the pitch DOF, d_h and d_α are the damping coefficients per unit length, $\bar{M}_\alpha = M_\alpha(mb^2\omega_h^2)^{-1}$ is the dimensionless pitch moment and $\bar{L} = L(mb\omega_h^2)^{-1}$ is the dimensionless lift force (Sousa and De Marqui Jr, 2014).

The dimensionless elastic moment due to the SMA springs, from Fig. 1(b), is

$$\vartheta\left(\alpha,\xi_1,\xi_2\right) = \frac{w}{mlb^2\omega_h^2}\left[-f_1^{\text{sma}}\left(\alpha,\xi_1\right) + f_2^{\text{sma}}\left(\alpha,\xi_2\right)\right] \tag{11}$$

where ξ_i is the martensitic fraction of each SMA spring (subscript i assumes 1 for S_1 and 2 for S_2) and w is the distance of each SMA spring from the elastic axis (Sousa and De Marqui Jr, 2014). The forces f_1^{sma} and f_2^{sma} of each SMA spring are

$$f_i^{\text{sma}} = k\left(\xi_i\right) y_i\left(\alpha\right) + Y\left(\xi_i\right), \quad i{=}\ 1\text{or}2 \tag{12}$$

where $y_i\left(\alpha\right)$ denotes the axial deflection of each SMA spring, which are approximated by

$$y_1\left(\alpha\right) = y_0 - w\alpha; \quad y_2\left(\alpha\right) = y_0 + w\alpha \tag{13}$$

and y_0 is the pre-deflection to the springs (preload) in order to bias the stresses towards the phase transformation region. The stiffness $k\left(\xi_i\right)$ of an SMA spring can be represented by

$$k\left(\xi_i\right) = \frac{r^4}{4R^3N}G\left(\xi_i\right) \tag{14}$$

where r is the coil spring wire radius, R is the mean coil radius, N is the number of active coils and $G\left(\xi\right)$ is the martensite-dependent shear modulus (Liang and Rogers, 1997). The shear modulus is given by

$$G\left(\xi_i\right) = G_A + \xi_i\left(G_M - G_A\right) \tag{15}$$

where G_M is the fully martensitic shear modulus and G_A is the fully austenitic shear modulus.

The inelastic term related to the hysteretic behavior in Eq. (12) is given by (Sousa and De Marqui Jr, 2014)

$$Y\left(\xi_i\right) = -\frac{\pi r^3}{2R}G\left(\xi_i\right)\xi_i\varepsilon_{\text{res}} \tag{16}$$

where ε_{res} is the maximum recoverable strain of the SMA.

The mechanical constitutive equation of Liang and Rogers (1997) for SMAs under pure torsion is used to represent the hysteretic shear stress-strain behavior. The initial state of the aeroelastic problem of this paper is known and thus the axial deflection of each SMA spring is computed at each time step as the numerical solution evolves. The corresponding shear strain of each SMA spring is estimated by

$$\gamma\left(y_i,\alpha\right) = \frac{r}{2\pi R^2N}y_i(\alpha) \tag{17}$$

which is used in $\tau = G\gamma$ in order to verify if the shear stress is within a transformation range. If so, the actual (nonlinear) shear stress is determined iteratively. Values for the shear stress in the transformation range (denoted by τ_{test}) are used in

Eq. (5) or (6) by considering the von Mises criterion for pure shear, $\sigma = \sqrt{3}\tau_{\text{test}}$ (Liang and Rogers, 1997). This yields in values for ξ_i between 0 and 1, denoted by ξ_{test}. Each pair $(\xi_{\text{test}},\ \tau_{\text{test}})$ is verified in the following equation

$$\tau_{\text{test}} - G\left(\xi_i\right)\left[\gamma\left(y_i, \alpha\right) - \xi_{\text{test}}\varepsilon_{\text{res}} + \theta\left(T - T_0\right)\right] = 0 \tag{18}$$

which also uses the shear strain obtained by Eq. (17) and where θ is related to the SMA thermal coefficient of expansion and T_0 is the SMA initial temperature (at the onset of the current phase transformation).

The state-space representation of the model is omitted here for brevity and can be found in Sousa and De Marqui Jr (2014).

3. RESULTS

SMA phase transformation parameters as well as thermal and electrical parameters are given in Tab. 1 (Hadi *et al.*, 2010; Aguiar *et al.*, 2013). The wire radius of the SMA springs is $r = 0.475\text{mm}$, the coil mean radius is $R = 4\text{mm}$ and the number of active coils is $N = 16.5$. The ambient temperature is assumed as $23\ ^\circ\text{C}$. For the given parameters and input voltage of $1.93\ \text{V}$, the steady-state temperature of the SMA springs is about $T = 58\ ^\circ\text{C}$ (equal to A_f). From Eq. (1) to (4), the corresponding critical stresses are $\tau_s^M = 95\text{MPa}$, $\tau_f^M = 135\text{MPa}$, $\tau_s^A = 52\text{MPa}$ and $\tau_f^A = 0\text{MPa}$. From Eq. (14), the fully austenitic stiffness of each SMA spring is $175\ \text{N} \cdot \text{m}^{-1}$. Moreover, the SMA springs are $36.7\ \text{mm}$ long and can be compressed up to $20\ \text{mm}$. The distance of each SMA spring from the elastic axis is $w = 85\text{mm}$. A fourth-order Runge-Kutta method with step size on the order of $10^{-6}\ \text{s}$ is used. The effect of thermal expansion on the overall aeroelastic response is negligible and is not discussed.

Table 1. SMA parameters (Hadi *et al.*, 2010; Aguiar *et al.*, 2013).

Parameter	Value	Unit
M_s	42	$^\circ\text{C}$
A_s	43	$^\circ\text{C}$
A_f	58	$^\circ\text{C}$
C_M	4	$\text{MPA} \cdot^\circ \text{C}^{-1}$
C_A	6	$\text{MPA} \cdot^\circ \text{C}^{-1}$
$\sigma_s^{\min}$	100	MPA
$\sigma_f^{\min}$	170	MPA
ε_{res}	0.067	$--$
G_M	11.5	GPa
G_A	14.5	GPa
θ	0.55	$\text{MPa} \cdot^\circ \text{C}^{-1}$
m_s	1.18×10^{-3}	kg
C_p	350	$\text{J} \cdot \text{kg}^{-1} \cdot^\circ \text{C}^{-1}$
L_h	6025	$\text{J} \cdot \text{kg}^{-1} \cdot^\circ \text{C}^{-1}$
R_A	0.7246	Ω
R_M	0.8197	Ω
h_c	150	$\text{J} \cdot \text{m}^{-2} \cdot^\circ \text{C}^{-1} \cdot \text{s}^{-1}$
A_c	9.77×10^{-4}	m^2

The aeroelastic parameters are given in Tab. 2 (Sousa *et al.*, 2011). An airfoil of $0.125\ \text{m}$ semichord length and $0.5\ \text{m}$ span length is assumed. An initial plunge displacement of $10\ \text{mm}$ is considered (or dimensionless plunge displacement of $\bar{h} = 0.08$) in all cases.

Table 2. Dimensionless aeroelastic parameters (Sousa *et al.*, 2011).

Parameter	Value
a	-0.5
c	0.5
μ	2.597
x_α	0.260
r_α	0.504
ζ_α	0.088
ζ_h	0.0035

Sousa and De Marqui Jr (2014) reported the effects of preloaded SMA springs on the aeroelastic response of a typical section oscillating at the flutter boundary as in Fig. 2. The amplitudes of oscillation decrease for preload values increasing from 2 N to 4.5 N. The effect of preload on the plunge and pitch amplitude is negligible for preload values greater than 3.5 N. Therefore, the case considering an intermediate preload value (3 N) is discussed in this paper.

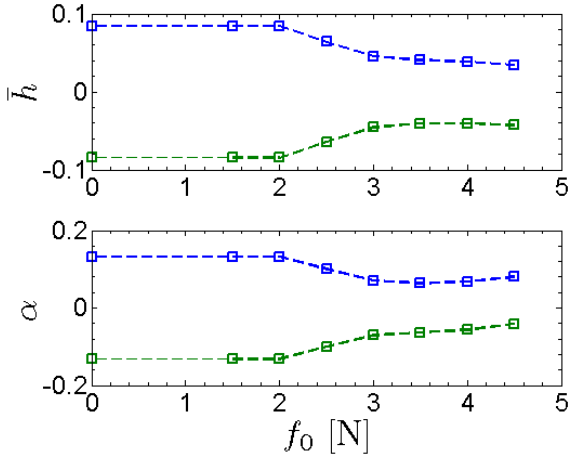

Figure 2. Aeroelastic peak displacements achieved at the flutter boundary for increasing preload values. Plunge (at the top half) and pitch (at the bottom half).

The aeroelastic behavior for two thermal boundary conditions (isothermal and non-isothermal assumptions) is described next. The plunge and pitch displacements are shown in Figs. 3(a) and (b) (only the positive peak values are shown for clarity). The steady-state pitch and plunge displacements for the airflow speed of 11.64 m/s and no preload are $\bar{h} \cong 0.08$ and $\alpha \cong 0.13$, respectively. This is the linear aeroelastic behavior since no phase transformation is achieved. The steady-state pitch and plunge for the airflow speed of 11.64 m/s and 3 N of preload are $\bar{h} \cong 0.04$ and $\alpha \cong 0.07$. The predicted attenuation is due to the pseudoelastic hysteresis of the SMAs. The steady-state pitch and plunge for the airflow speed of 14 m/s and 3 N of preload are $\bar{h} \cong 0.14$ and $\alpha \cong 0.17$. The persistent oscillations under post-flutter regime (limit cycle oscillations) are also due to the hysteresis of the SMAs. The non-isothermal assumption yields slightly larger aeroelastic displacements for the airflow speed of 14 m/s (α increases less than 0.01 radians) while in the other cases the effect is negligible.

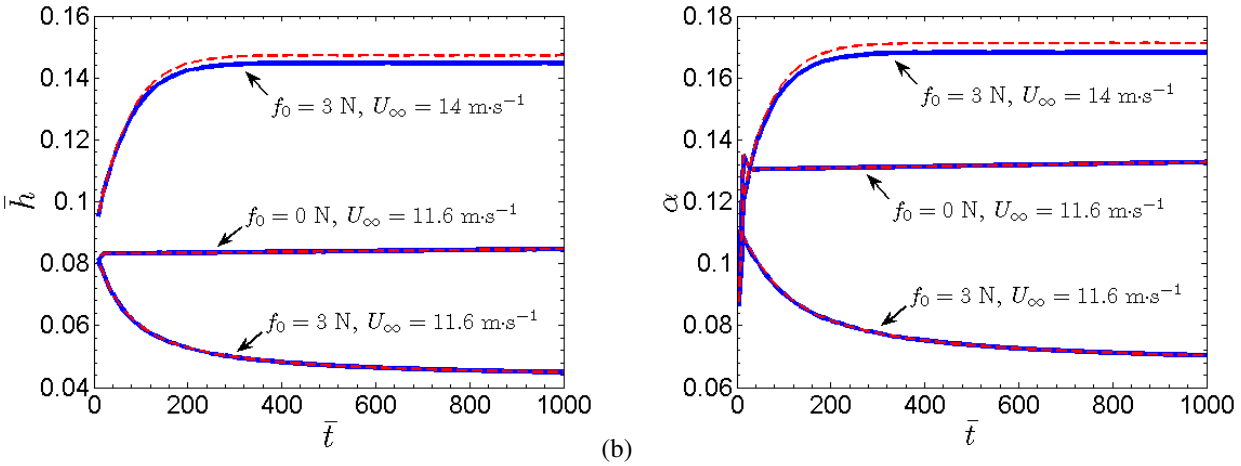

(a) (b)

Figure 3. (a) Plunge and (b) pitch aeroelastic displacements (continuous lines: isothermal; dashed lines: non-isothermal).

The behavior of the SMA springs for the same case studies above is discussed next. For brevity, only SMA spring S_1 (please check Fig. 1(b)) is addressed, but spring S_2 behaves very similarly. Figure 4(a) shows the elongation of the SMA spring, which has contributions of preload (yielding in pre-deflection) and pitch displacement. Figure 4(b) shows the corresponding shear stress. Figure 4(c) shows the shear stress against elongation and Fig. 4(d) shows a detail of the martensitic plateau of the third plot of Fig. 4(c). Figure 4(e) represents the martensitic fraction. Figures 4(f) and (g) represent the stiffness and electrical resistance, respectively. Continuous lines are isothermal and dashed lines are non-isothermal cases.

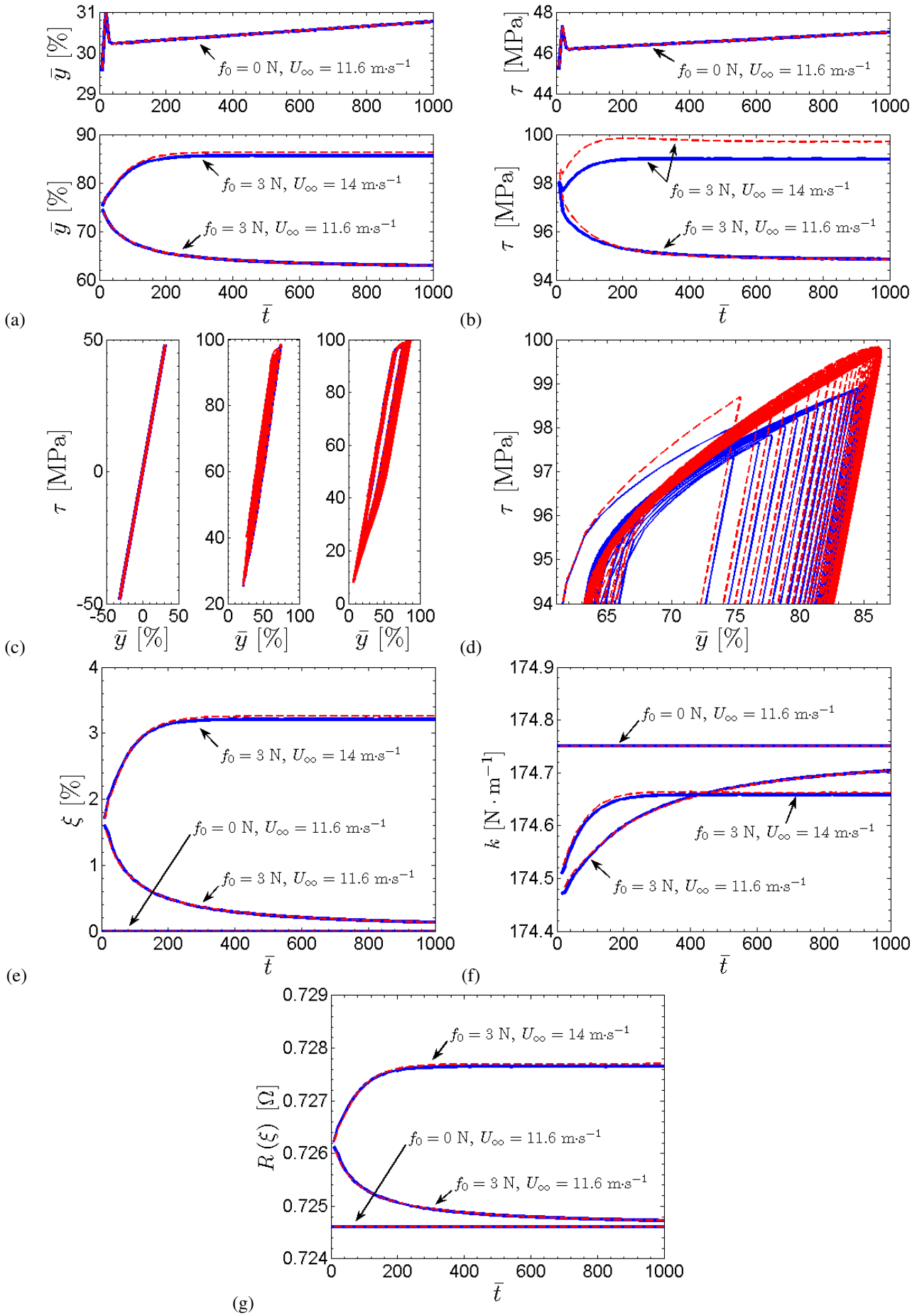

Figure 4. Behavior of the SMA springs: (a) elongation, (b) shear stress, (c) shear stress-elongation diagrams, (d) detail of the diagram for 14 m/s, (e) martensite volumetric fraction, (f) stiffness, (g) electrical resistance and (h) temperature. Continuous lines are isothermal and dashed lines are non-isothermal.

The variation of temperature for each case study of Figs. 3 is shown in Fig. 5(a). For 3 N of preload (either at 11.64 m/s or 14 m/s) the average temperature slightly drops below the initial temperature (despite the isothermal assumption) because of the increase in the electrical resistivity related to the martensitic phase. At 14 m/s (for the non-isothermal assumption) the average temperature is above the initial temperature due to the latent heat. The change in temperature affects the critical stresses, resulting in the higher position of the hysteresis loop shown in Fig. 4(d). The critical stress for the onset of forward phase transformation (τ_s^M) is shown in Fig. 5(b). The variations in temperature and critical stresses are small since the phase transformations take place for short periods, yielding low martensite fraction (as shown in Fig. 4(e)).

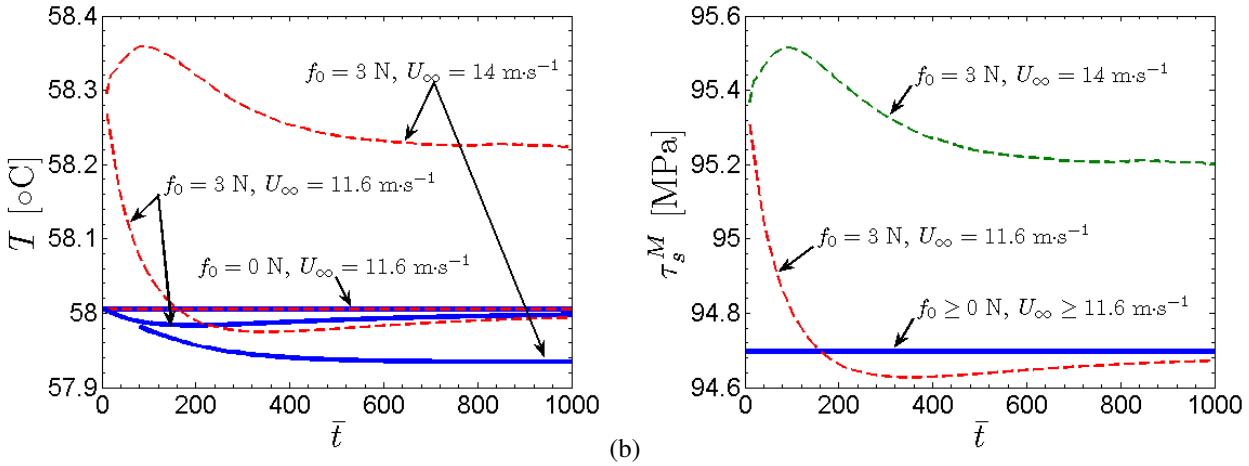

(a) (b)

Figure 5. Temperature variations (a) and the corresponding critical stress τ_s^M (b). Continuous line is isothermal and dashed lines are non-isothermal.

4. CONCLUSIONS

The aeroelastic behavior of a 2-DOF typical airfoil section with SMA springs is discussed. The SMA springs are modeled in the pitch DOF and the most influential thermal effects are of concern. The unsteady aerodynamic loads are represented by an augmented-state model. The nonlinear model is cast in state-space representation and solved in time domain. The effect of preloading the SMA springs on the aeroelastic behavior at the flutter boundary and above is investigated. The results show that the isothermal assumption could be an acceptable hypothesis for the cases presented here. However, temperature effects could be much more influential for different models or case studies and hence should be accounted for in proper SMA modeling.

5. ACKNOWLEDGEMENTS

This work was supported by the São Paulo Research Foundation (FAPESP) [grant numbers 2015/26045-6 and 2017/08467-6]; and the CAPES Foundation (Brazilian Federal Agency for Support and Evaluation of Graduate Education) [grant number DS-00011/07-0].

6. REFERENCES

Aguiar, R.A.A., Leão Neto, W.C.C., Savi, M.A. and Pacheco, P.M.C.L., 2013. "Shape memory alloy helical springs performance: modeling and experimental analysis". *Materials Science Forum*, Vol. 758, pp. 147–156. doi: 10.4028/www.scientific.net/MSF.758.147. URL `http://www.scientific.net/MSF.758.147`.

Brinson, L., 1993. "One-Dimensional Constitutive Behavior of Shape Memory Alloys: Thermomechanical Derivation with Non-Constant Material Functions and Redefined Martensite Internal Variable". *Journal of Intelligent Material Systems and Structures*, Vol. 4, No. 2, pp. 229–242. ISSN 1045-389X. doi:10.1177/1045389X9300400213. URL `http://jim.sagepub.com/cgi/doi/10.1177/1045389X9300400213`.

Edwards, J.W., 1977. "Unsteady aerodynamic modeling and active aeroelastic control". URL `http://hdl.handle.net/2060/19780002074`.

Faulkner, M.G., Amalraj, J.J. and Bhattacharyya, A., 2000. "Experimental determination of thermal and electrical properties of Ni-Ti shape memory wires". *Smart Materials and Structures*, Vol. 9, No. 5, pp. 632–639. doi:10.1088/0964-1726/9/5/307. URL `https://doi.org/10.1088/0964-1726/9/5/307`.

Gandhi, F.S. and Chapuis, G., 2002. "Passive damping augmentation of a vibrating beam using pseudoelastic shape memory alloy wires". *Journal of Sound and Vibration*, Vol. 250, No. 3, pp. 519–539. ISSN 0022460X. doi:

10.1006/jsvi.2001.3935. URL http://linkinghub.elsevier.com/retrieve/pii/S0022460X01939355.

Giurgiutiu, V., 2000. "Review of smart-materials actuation solutions for aeroelastic and vibration control". *Journal of Intelligent Material Systems and Structures*, Vol. 11, No. 7, pp. 525–544. ISSN 1045389X. doi:10.1106/HYTV-NC7R-BCMM-W3CH. URL http://jim.sagepub.com/cgi/doi/10.1106/HYTV-NC7R-BCMM-W3CH.

Hadi, A., Yousefi-Koma, A., Moghaddam, M.M., Elahinia, M.H. and Ghazavi, A., 2010. "Developing a novel SMA-actuated robotic module". *Sensors and Actuators A: Physical*, Vol. 162, No. 1, pp. 72–81. ISSN 09244247. doi:10.1016/j.sna.2010.06.014. URL http://linkinghub.elsevier.com/retrieve/pii/S092442471000275X.

Ibrahim, R., 2008. "Recent advances in nonlinear passive vibration isolators". *Journal of Sound and Vibration*, Vol. 314, No. 3-5, pp. 371–452. ISSN 0022460X. doi:10.1016/j.jsv.2008.01.014. URL http://linkinghub.elsevier.com/retrieve/pii/S0022460X08000436.

Jones, R.T., 1938. "Operational treatment of the nonuniform-lift theory in airplane dynamics". Technical report, N.A.C.A. Technical Note 667. Washington.

Liang, C. and Rogers, C.A., 1997. "Design of shape memory alloy springs with applications in vibration control". *Journal of Intelligent Material Systems and Structures*, Vol. 8, No. 4, pp. 314–322. doi:10.1177/1045389X9700800404. URL http://jim.sagepub.com/cgi/doi/10.1177/1045389X9700800404.

Sousa, V.C., de M Anicézio, M., De Marqui Jr, C. and Erturk, A., 2011. "Enhanced aeroelastic energy harvesting by exploiting combined nonlinearities: theory and experiment". *Smart Materials and Structures*, Vol. 20, No. 9, p. 094007. ISSN 0964-1726. doi:10.1088/0964-1726/20/9/094007. URL stacks.iop.org/SMS/20/094007.

Sousa, V.C. and De Marqui Jr, C., 2014. "Effect of pseudoelastic hysteresis of shape memory alloy springs on the aeroelastic behavior of a typical airfoil section". *Journal of Intelligent Material Systems and Structures*, Vol. 27, No. 1, pp. 117–133. ISSN 1045-389X. doi:10.1177/1045389X14563862. URL http://jim.sagepub.com/cgi/doi/10.1177/1045389X14563862.

7. RESPONSIBILITY NOTICE

The authors are the only responsible for the printed material included in this paper.